

# Scalable Seashell-Based Chemical Vapor Deposition Growth of Three-Dimensional Graphene Foams for Oil–Water Separation

Liurong Shi,<sup>†</sup> Ke Chen,<sup>†</sup> Ran Du,<sup>†</sup> Alicja Bachmatiuk,<sup>‡,‡</sup> Mark Hermann Rummeli,<sup>‡,§</sup> Kongwei Xie,<sup>||</sup> Youyuan Huang,<sup>||</sup> Yanfeng Zhang,<sup>\*,†,⊥</sup> and Zhongfan Liu<sup>\*,†</sup>

<sup>†</sup>Center for Nanochemistry (CNC), Beijing Science and Engineering Center for Nanocarbons, Beijing National Laboratory for Molecular Sciences, College of Chemistry and Molecular Engineering, Peking University, Beijing 100871, P. R. China

<sup>‡</sup>Centre of Polymer and Carbon Materials, Polish Academy of Sciences, M. Curie-Sklodowskiej 34, Zabrze 41-819, Poland

<sup>#</sup>IFW Dresden, 20 Helmholtz Strasse, Dresden 01069, Germany

<sup>§</sup>School of Energy, Soochow University, Suzhou 215006, P. R. China

<sup>||</sup>BTR New Energy Materials Inc., Shenzhen 518106, P. R. China

<sup>⊥</sup>Department of Materials Science and Engineering, College of Engineering, Peking University, Beijing 100871, P. R. China

## Supporting Information

**ABSTRACT:** A seashell-based CVD technique for preparing three-dimensional (3D) graphene foams is reported. The graphene sheets in thus-obtained foams are seamlessly interconnected into a 3D flexible network, forming highly porous materials with negligible non-carbon impurities, ultralow density, and outstanding mechanical flexibility and electrical conductivity. These 3D graphene foams demonstrate a fast adsorption performance toward various oils and organic solvents, with adsorption capacity up to 250-fold weight gain. The present approach offers a practical route for scalable construction of 3D graphene foams for versatile applications such as energy storage and water remediation.

Three-dimensional (3D) graphene foam, a combination of two-dimensional (2D) graphene building blocks and 3D porous structures, has attracted significant attention in recent years.<sup>1–3</sup> Such graphene foams are self-supporting materials, possessing the fascinating intrinsic properties of graphene together with high porosity and ultralow density. A number of approaches such as sol–gel process and template growth have been reported for fabricating 3D graphene foams.<sup>1–6</sup> Sol–gel process of graphene oxide usually creates materials with abundant structural defects, chemical impurities, and discontinuous interconnections between individual graphene sheets arising from the solution process. Therefore, serious degradation of the intrinsic properties of graphene such as electron and phonon transports is seen. Template-assisted chemical vapor deposition (CVD) provides an effective way to synthesize 3D graphene foams composed of seamless interconnected graphene sheets with high purity and quality.<sup>1</sup> For instance, graphene foams grown from a nickel foam template have demonstrated excellent mechanical strength and superior electrical conductivity.<sup>1,7,8</sup> However, intrinsic drawbacks exist in this approach, including the time-consuming template removal process, unavoidable metal residues, and limited choice of metal foams and their microstructures. For practical applications, cost should also be taken into account. Obviously,

mass production of 3D graphene foams in this way would consume great amounts of expensive nickel metals.

It is extremely attractive to develop low-cost and easily removable CVD growth templates for industrial fabrication of 3D graphene foams. In light of this, we turned our attention to natural seashells, the highly abundant shells of oceanic mollusks. The main chemical composition of seashells is calcium carbonate.<sup>9</sup> Depending on the source mollusks, seashells have versatile microscopic structures. Furthermore, a simple chemical calcination can easily convert the biological calcium carbonate into calcium oxide without destroying the structural framework, and then the calcium oxide can be readily washed away with dilute acid. In this work, we demonstrate the CVD template function of seashells for fabricating 3D graphene foams for the first time. Scallop, which is produced in massive amounts worldwide, was employed as a typical example for demonstration.<sup>10</sup> In this way, graphene foams with high purity, high porosity, ultralow density, and superior bendability have been synthesized. More interestingly, bespoke shape control of such graphene foams can be easily achieved through the lime slaking process of calcium oxide. Notably, the present approach could also be extended to other seashells, offering great opportunities for controlling the microscopic structures of graphene foams. By virtue of their unique structures and properties, applications of obtained graphene foams as binder-free Li-ion battery anodes and oil adsorbents have been demonstrated.

The procedure for fabrication of 3D graphene foam using scallop template is shown in Figure 1a. Scallop, a naturally abundant biomass, is composed of calcium carbonate (95 vol%) and organic biopolymers (5 vol%).<sup>11</sup> Inside the scallop, the architecture resembles a 3D brick-and-mortar wall at the mesoscale level<sup>11</sup> (Figure 1b). However, the tight packing of the calcium carbonate is not suitable for direct CVD growth of graphene foams since carbon species cannot effectively enter into the pores, which is required for graphene growth. When

Received: March 1, 2016

Published: May 9, 2016

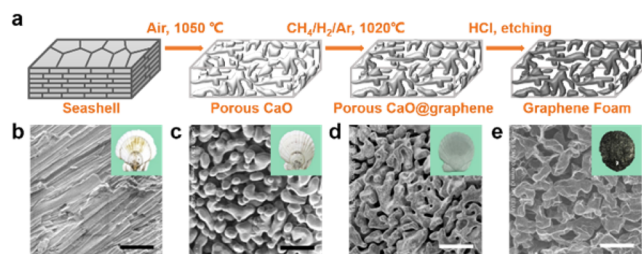


**Figure 1.** Fabrication of scallop-derived 3D graphene foams. (a) Schematic illustration of graphene foam formation. SEM images of (b) pristine scallop microstructure, (c) scallop calcined at 1050 °C for 30 min in air, (d) graphene-coated calcined scallop after CVD growth at 1020 °C for 30 min, and (e) 3D graphene foam after removal of the CaO framework. Insets of panels b–e are the corresponding photographs. All the scale bars are 5  $\mu\text{m}$ .

heated in air, the organic molecules and  $\text{CaCO}_3$  in scallop start to decompose, with releasing  $\text{CO}_2$  gas. This leads to an interconnected porous structure within the scallop bulk while keeping the scallop framework unchanged (Figure 1c). At the same time,  $\text{CaCO}_3$  inside the scallop shell fully converts to CaO following the reaction below<sup>12</sup> (Figure S1):



Thus-obtained highly porous CaO framework was then heated to 1020 °C for graphene growth under a mixed-gas atmosphere ( $\text{CH}_4:\text{H}_2:\text{Ar} = 10:30:300$  sccm) for 0.5–2 h. During this process, graphene layers were deposited on the CaO surface, forming CaO@graphene structure (Figure 1d). In this case, it is proposed that the oxygen atoms on the surface of the CaO template could exert a synergistic effect on the graphene synthesis, i.e., by enhancing the absorption and decomposition of hydrocarbons at high temperature and promoting the carbon–carbon coupling on the substrate.<sup>13,14</sup> After etching in dilute hydrochloric acid, a self-supporting 3D graphene foam was obtained by a freeze-drying treatment (Figure S2). As can be seen from the scanning electron microscopy (SEM) image (Figure 1e), thus-formed graphene foam well inherited the interconnected microstructure of original CaO template.

The quality of as-grown graphene was systematically investigated (Figures S3 and S4). Because the graphene foams are curved with a porous structure, it is difficult to use Raman mapping to evaluate the quality of graphene over a large area. Figure 2a shows six randomly selected Raman spectra from different spatial locations of the graphene foams grown at 1020 °C for 120 min. Identical  $I_{\text{D}}/I_{\text{G}}$  ratio (0.86) and fwhm of the 2D peak ( $80 \text{ cm}^{-1}$ )<sup>15</sup> confirmed the uniformity of the foam at macroscopic scale. A typical C 1s X-ray photoelectron spectroscopy (XPS) spectrum of thus-prepared graphene foam can be fitted with two signals from graphene, a major  $\text{sp}^2$  carbon peak at 284.4 eV and a very small C–H peak at 285.3 eV (Figure 2b), suggesting considerably small non-carbon impurities.<sup>16</sup> To further evaluate the crystalline quality of graphene foam, sonication in ethanol was performed, followed by dropping onto a copper grid for transmission electron microscopy (TEM) analysis. The low-magnification TEM image shows a crumpled and electron-transparent feature (Figure 2c). The corresponding selective area electron diffraction (SAED) pattern (inset in Figure 2c) is composed of four sets of hexagonal symmetric patterns, indicative of graphene domains with different orientations. Figure 2d shows

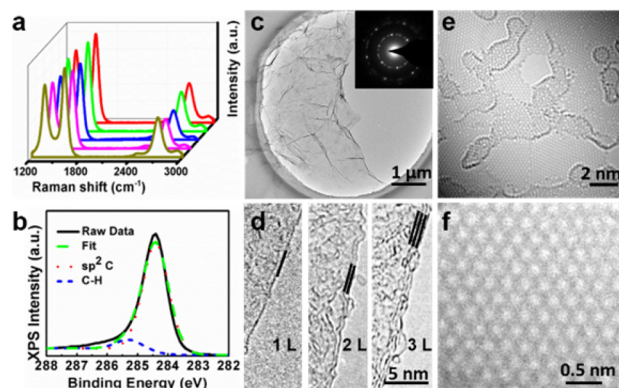


**Figure 2.** Spectroscopic and structural characterization of graphene foams. (a) Raman spectra observed at different locations in a large area. (b) C 1s XPS spectrum of graphene foam. (c) TEM image of graphene sheet; inset is the corresponding SEAD pattern. (d) High-resolution TEM images of as-grown graphene sheets with different layer numbers. (e, f) Atomic resolution, aberration-corrected TEM images of graphene foam.

layer numbers ranging from 1 to 3 layers. As shown in Figure 2e, the graphene sheet is composed of domains with different orientations having single crystalline domain sizes of 2–10 nm.<sup>17</sup> A magnified image from a single domain clearly reveals the graphene atomic structure with a lattice constant of  $\sim 0.246 \text{ nm}$  (Figure 2f).

The porous microstructure of CaO template calcined from scallop was found to be very stable in a wide experimental window. When the heating rate of scallop calcination was varied from 5, to 15, to 25 °C/min, the morphology of CaO@graphene remained the same, as shown in Figure 3a, giving an average pore size of  $\sim 300 \text{ nm}$  and an average branch width of  $\sim 1 \mu\text{m}$ . Similar results were also observed when changing the calcination temperature (850, 950, and 1050 °C) (Figure 3b) as

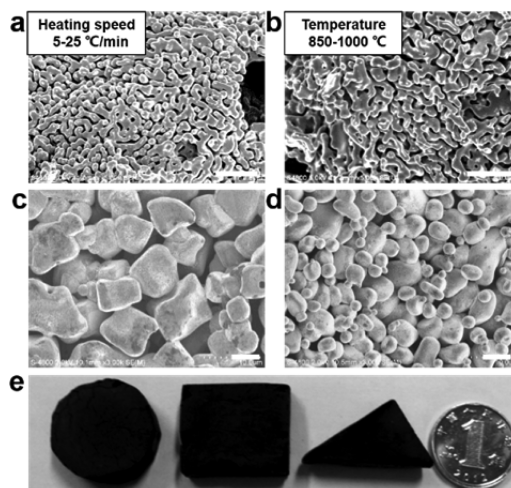


**Figure 3.** Morphology control of calcined seashells and graphene foams. (a) Typical SEM image of CaO@graphene with different heating rates for calcination of scallop (5, 15, and 25 °C/min). (b) SEM image of CaO@graphene obtained with different calcination temperatures (850, 950, and 1050 °C). SEM images of CaO@graphene obtained from (c) conch and (d) starfish (calcination at 1050 °C for 0.5 h, heating rate 25 °C/min). (e) Graphene foams with different shapes and sizes made from scallop by using the lime slaking reaction. All scale bars are 5  $\mu\text{m}$ .

well as the calcination atmosphere (Figure S5). This structural stability with varying experimental condition changes is important for mass production of 3D graphene foams with uniform macroscopic performance.

We extended our scallop-based approach to other seashells such as conch and starfish. Figure 3c,d exhibits the SEM images of graphene-coated CaO obtained by using conch and starfish instead of scallop, respectively. Obviously, the porous microstructures from conch and starfish are much larger than that of scallop. Especially for the conch-derived microstructure, the average pore size is about 10 times larger than the scallop case. This clearly shows the freedom of structural design of the biomass-derived 3D graphene foams.

CaO can react very easily with water, a process known as lime slaking. Hereby, the graphene foams can be molded into arbitrary shapes macroscopically. Figure 3e exhibits three differently shaped graphene foams made from scallop in such a way. More interestingly, the molding process might be utilized to manipulate the morphology of the CaO substrate and thus tailor the microstructures and corresponding properties of the graphene foams (Figure S6). In this regard, CaO can serve as an effective substrate for the growth of structure-controllable graphene materials. Different from previously reported CaO-assisted CVD-grown graphene powder,<sup>18</sup> the present approach provides an efficient way to prepare free-standing graphene monoliths, capable of extending their applications to binder-free electrodes for electronic devices, as well as self-supporting scaffolds for catalysts and stem cells, etc.

The self-supporting 3D graphene foams fabricated by the scallop-based CVD approach have extremely low density,  $\sim 3$  mg/cm<sup>3</sup> (Figure 4a). They also exhibit excellent flexibility, as

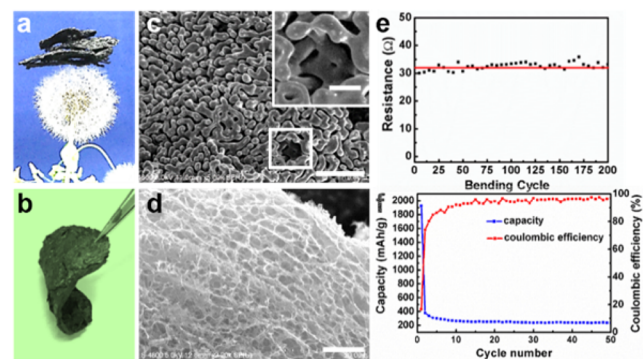


**Figure 4.** Mechanical bendability and its origin. Photographs of (a) ultralight graphene foams resting on a dandelion and (b) flexible graphene foam. (c) SEM image of CaO@graphene showing layer-by-layer arrangement; inset is a zoom-in of the marked region. (d) Cross-section view SEM image of graphene foam with layered structure. (e) Resistance change of graphene foam over 200 bending cycles. (f) Discharge capacity and coulombic efficiency of the binder-free flexible anode for a lithium-ion battery at 50 mA/g, 2 V vs Li<sup>+</sup>/Li. Scale bar for (c) is 5  $\mu$ m, for inset in (c) is 2  $\mu$ m, and for (d) is 10  $\mu$ m.

shown in Figure 4b, with no breaking or cracking observed over repeated bending. These excellent performance qualities are attributed to the highly porous and interconnected structures inherited from the calcined scallop. As can be seen in Figure 4c,d, after calcination and CVD, CaO@graphene maintained the major layered structure along with the presence of interconnected pores. As a result, the cross-section SEM image of the resultant graphene foam showed a layered arrangement (Figure 4d).

The mechanical durability of materials is an important factor for flexible electronics. It can be seen from Figure 4e that there was no significant change in the electrical resistance over 200 mechanical bending cycles, which might be attributed to the layered arrangement,<sup>19</sup> the curved surfaces, and the branched structure<sup>20</sup> of the graphene foam (Figures S7 and S8). In addition, the as-obtained graphene foam can be used directly as a binder-free anode for flexible energy storage devices. As shown in Figure 4f, the Li-ion battery assembled from the current graphene foam had a capacity of  $\sim 260$  mAh/g with  $\sim 95\%$  coulombic efficiency after 50 charge–discharge cycles, which is comparable with that of nickel foam-derived graphene foam (200 mAh/g after 20 cycles<sup>21</sup>). It is worth noting that, although the energy storage performance of such graphene foams is relatively lower than that of certain prepared graphene materials,<sup>22–24</sup> it may be considerably improved by adopting effective strategies like heteroatom doping and structure optimization reported elsewhere.<sup>22</sup>

Our seashell-derived 3D graphene foam contains much less non-carbon species as compared with those made from wet chemistry techniques. It is therefore an excellent material for oil–water separation.<sup>25</sup> Figure 5a demonstrates the rapid

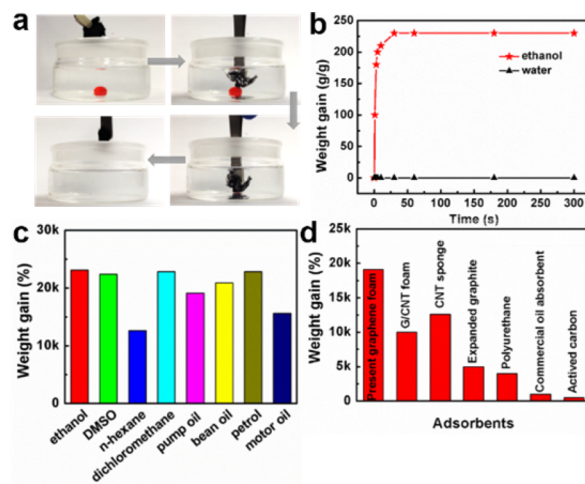


**Figure 5.** Organic solvents and oil adsorption performance of 3D graphene foams. (a) Demonstration of methylene chloride (dyed with Sudan III) adsorption from water by using a piece of graphene foam. (b) Adsorption kinetics of ethanol and water using graphene foam. (c) Adsorption capacity of different substances using graphene foams. (d) Adsorption capacities of different carbon-based materials for pump oil.<sup>26–28</sup>

sucking-up process of methylene chloride dyed with Sudan III into 3D graphene foam. Within 2 s, 132.5 mg of methylene chloride was swallowed by a piece of graphene foam from water. Figure 5b shows the fast adsorption kinetics of ethanol using the graphene foams.<sup>25</sup> The zero adsorption capacity of water indicates the hydrophobic nature of the graphene foam. Such excellent adsorption performance of the graphene foams was observed in a wide range of organic liquids, including common pollutants such as ethanol, DMSO, *n*-hexane, dichloromethane, pump oil, bean oil, petrol, and motor oil (Figure 5c). The adsorption capacity of the biomass-derived 3D graphene foams can reach up to 200–250 times its own weight. This is much higher than other typical carbonaceous sorbents previously reported for pump oil<sup>26–28</sup> (Figure 5d). The high oil adsorption capacity benefits predominantly from the low

density of the graphene foams (Figure S9). The practical adsorption capacity depends on the density, viscosity, and surface tension of the oils. It should be emphasized that the adsorbates can be easily removed by exchange with acetone, indicating the recyclability of the graphene foam.

In summary, we have developed a seashell-based CVD growth technique for graphene foams with diverse morphologies. The abundance of biomass and its easy removability make the production process scalable and low-cost. The seashell-derived 3D graphene foams exhibited outstanding mechanical flexibility and electrical conductivity with negligible non-carbon impurities. By using these graphene foams, a binder-free, flexible Li-ion battery was made with a capacity of 260 mAh/g. The graphene foams also demonstrated fast adsorption of various oils and organic solvents, with an adsorption capacity up to 250-fold weight gain. We believe the approach presented here offers a practical route for scalable production of graphene foams with wide applications including energy storage, water remediation, etc.

## ■ ASSOCIATED CONTENT

### 📄 Supporting Information

The Supporting Information is available free of charge on the ACS Publications website at DOI: 10.1021/jacs.6b02262.

Experimental details and additional description, characterizations, and data analysis, including Figures S1–S9 (PDF)

## ■ AUTHOR INFORMATION

### Corresponding Authors

\*yanfengzhang@pku.edu.cn

\*zliu@pku.edu.cn

### Notes

The authors declare no competing financial interest.

## ■ ACKNOWLEDGMENTS

This work was financially supported by the Ministry of Science and Technology of China (Grants 2013CB932603, 2012CB-933404), the National Natural Science Foundation of China (Grants 51520105003, 51432002, 51290272), and the Beijing Municipal Science and Technology Planning Project (Z1511-0000335013; Z141103004414103).

## ■ REFERENCES

- (1) Chen, Z.; Ren, W.; Gao, L.; Liu, B.; Pei, S.; Cheng, H.-M. *Nat. Mater.* **2011**, *10*, 424.
- (2) Qiu, L.; Liu, J. Z.; Chang, S. L. Y.; Wu, Y.; Li, D. *Nat. Commun.* **2012**, *3*, 1241.
- (3) Hong, J.-Y.; Bak, B. M.; Wie, J. J.; Kong, J.; Park, H. S. *Adv. Funct. Mater.* **2015**, *25*, 1053.
- (4) Zhao, Y.; Liu, J.; Hu, Y.; Cheng, H. H.; Hu, C. G.; Jiang, C.; Jiang, L.; Cao, A.; Qu, L. *Adv. Mater.* **2013**, *25*, 591.
- (5) Liang, Y.; Li, Y.; Wang, H.; Zhou, J.; Wang, J.; Regier, T.; Dai, H. *Nat. Mater.* **2011**, *10*, 780.
- (6) Yavari, F.; Chen, Z.; Thomas, A. V.; Ren, W.; Cheng, H.-M.; Koratkar, N. *Sci. Rep.* **2011**, *1*, 166.
- (7) Ito, Y.; Qiu, H. J.; Fujita, T.; Tanabe, Y.; Tanigaki, K.; Chen, M. *Adv. Mater.* **2014**, *26*, 4145.
- (8) Ito, Y.; Tanabe, Y.; Qiu, H. J.; Sugawara, K.; Heguri, S.; Tu, N. H.; Huynh, K. K.; Fujita, T.; Takahashi, T.; Tanigaki, K.; Chen, M. *Angew. Chem., Int. Ed.* **2014**, *53*, 4822.
- (9) Wang, J.; Cheng, Q.; Lin, L.; Jiang, L. *ACS Nano* **2014**, *8*, 2739.

- (10) Buasri, A.; Chaiyut, N.; Loryuenyong, V.; Worawanitchaphong, P.; Trongyong, S. *Sci. World J.* **2013**, *2013*, 460923.
- (11) Wang, J.; Cheng, Q.; Tang, Z. *Chem. Soc. Rev.* **2012**, *41*, 1111.
- (12) Sirisomboonchai, S.; Abuduwayiti, M.; Guan, G.; Samart, C.; Abliz, S.; Hao, X.; Kusakabe, K.; Abudula, A. *Energy Convers. Manage.* **2015**, *95*, 242.
- (13) Chen, J.; Wen, Y.; Guo, Y.; Wu, B.; Huang, L.; Xue, Y.; Geng, D.; Wang, D.; Yu, G.; Liu, Y. *J. Am. Chem. Soc.* **2011**, *133*, 17548.
- (14) Sun, J.; Gao, T.; Song, X.; Zhao, Y.; Lin, Y.; Wang, H.; Ma, D.; Chen, Y.; Xiang, W.; Wang, J.; Zhang, Y.; Liu, Z. *J. Am. Chem. Soc.* **2014**, *136*, 6574.
- (15) Ferrari, A. C.; Basko, D. M. *Nat. Nanotechnol.* **2013**, *8*, 235.
- (16) Chen, Y.; Sun, J.; Gao, J.; Du, F.; Han, Q.; Nie, Y.; Chen, Z.; Bachmatiuk, A.; Priyadarshi, M. K.; Ma, D.; Song, X.; Wu, X.; Xiong, C.; Rummeli, M. H.; Ding, F.; Zhang, Y.; Liu, Z. *Adv. Mater.* **2015**, *27*, 7839.
- (17) Rasool, H. I.; Ophus, C.; Zettl, A. *Adv. Mater.* **2015**, *27*, 5771.
- (18) Tang, C.; Li, B.-Q.; Zhang, Q.; Zhu, L.; Wang, H.-F.; Shi, J.-L.; Wei, F. *Adv. Funct. Mater.* **2016**, *26*, 577.
- (19) Gwon, H.; Kim, H.-S.; Lee, K. U.; Seo, D.-H.; Park, Y. C.; Lee, Y.-S.; Ahn, B. T.; Kang, K. *Energy Environ. Sci.* **2011**, *4*, 1277.
- (20) Yin, J.; Li, X.; Zhou, J.; Guo, W. *Nano Lett.* **2013**, *13*, 3232.
- (21) Luo, J.; Liu, J.; Zeng, Z.; Ng, C.; Ma, L.; Zhang, H.; Lin, J.; Shen, Z.; Fan, H. *Nano Lett.* **2013**, *13*, 6136.
- (22) Wang, Z.; Xu, D.; Wang, H.; Wu, Z.; Zhang, X. *ACS Nano* **2013**, *7*, 2422.
- (23) Hassoun, J.; Bonaccorso, F.; Agostini, M.; Angelucci, M. G.; Betti, M.; Cingolani, R.; Gemmi, M.; Mariani, C.; Panero, S.; Pellegrini, V.; Scrosati, B. *Nano Lett.* **2014**, *14*, 4901.
- (24) Lian, P.; Zhu, X.; Liang, S.; Li, Z.; Yang, W.; Wang, H. *Electrochim. Acta* **2010**, *55*, 3909.
- (25) Du, R.; Zhang, N.; Xu, H.; Mao, N.; Duan, W.; Wang, J.; Zhao, Q.; Liu, Z.; Zhang, J. *Adv. Mater.* **2014**, *26*, 8053.
- (26) Dong, X.; Chen, J.; Ma, Y.; Wang, J.; Chan-Park, M. B.; Liu, X.; Wang, L.; Huang, W.; Chen, P. *Chem. Commun.* **2012**, *48*, 10660.
- (27) Sohn, K.; Na, Y. J.; Chang, H.; Roh, K.-M.; Jang, H. D.; Huang, J. *Chem. Commun.* **2012**, *48*, 5968.
- (28) Bi, H.; Xie, X.; Yin, K.; Zhou, Y.; Wan, S.; He, L.; Xu, F.; Banhart, F.; Sun, L.; Ruoff, R. S. *Adv. Funct. Mater.* **2012**, *22*, 4421.